# Standalone L4-L5 Extreme Lateral Interbody Fusion: An examination of the influence of bone graft stiffness characteristics on load distribution in the spinal column using finite element modelling

Vivek A.S. Ramakrishna[1,2,3], Uphar Chamoli*[2,4], Subhas C. Mukhopadhyay[3], B. Gangadhara Prusty[1], Ashish D. Diwan[2,6]

1. School of Mechanical and Manufacturing Engineering, University of New South Wales, Sydney, Kensington, New South Wales, Australia.

2. Spine Labs, St. George & Sutherland Clinical School, University of New South Wales, Sydney, New South Wales, Australia

3. School of Engineering, Faculty of Science and Engineering, Macquarie University, Sydney, New South Wales, Australia

4. School of Biomedical Engineering, Faculty of Engineering and Information Technology, University of Technology Sydney, Ultimo, New South Wales, Australia

5. Spine Service, Department of Orthopaedic Surgery St. George Hospital Campus, Kogarah, New South Wales, Australia.


*Corresponding author: Uphar Chamoli, PhD

Level 3, WR Pitney Building, St. George & Sutherland Clinical School

The University of New South Wales, Kogarah, NSW 2217

Phone: + 61 2 8566 7166

Fax: +61 2 8566 7177

Email: u.chamoli@unsw.edu.au

**Introduction**

Lumbar interbody fusion (LIF) is a common approach for the treatment of degenerative and instability-inducing conditions of the spine. Extreme Lateral Interbody Fusion (XLIF) was introduced as a minimally disruptive alternative to the anterior approach, allowing for the insertion of a large-footprint interbody cage through trans-psoas retroperitoneal access [1, 2]. XLIF maintains a theoretical advantage over anterior, posterior, and transforaminal approaches by preserving the stabilising capacity of the facets, anterior longitudinal ligament, and posterior ligaments [1]. The additional abutment provided by the ligaments under tension allows surgeons to consider implanting a standalone XLIF cage without supplemental lateral or posterior fixation [1, 3]. Hence, standalone XLIF without supplemental fixation represent 25% - 33% of all XLIF surgeries [4, 5].

Very little is known about temporal bone graft stiffness changes *in vivo* for lumbar interbody fusion. Part of the biomechanical optimisation of interbody cages includes the assessment of stress-shielding and loading characteristics in the graft region [6]. Load-sharing patterns in the cage region are of particular interest when analysing the progression to solid bony union with respect to Wolff's law [7]. The biomechanical effects of bone graft stiffness changes until complete fusion is reached are not well-understood. Previous finite element (FE) analysis studies have shown increased load on bone graft with increasing stiffness [8, 9] as a motion segment progresses to complete fusion. Further, Vadapalli et al. demonstrated superior load transfer through the graft with a Polyether ether ketone (PEEK) interbody cage compared to titanium, with the more mechanically compliant PEEK cage material allowing a better load-share between the cage and graft [10]. A thorough *in vitro* analysis of load-transfer with different cage configurations was undertaken by Du et al., demonstrating increased cage loading with cage height, however results from the graft region were not reported [11]. It remains unclear how temporal graft changes impact load-sharing in the context of surrounding spinal structures. Comparison of load-sharing through the cage and graft is incomplete without consideration of the ligaments and facets, particularly in an XLIF setting.

The temporal features of biological bone growth following LIF surgery have not yet been adequately modelled. Stiffness of the fusion bone is known to increase during the healing process [8], most likely from the soft callus to the cancellous or cortical stage according to natural bone formation pathways. During early stages of bone formation, bonding to the endplates is not complete, whereas after complete fusion, the newly formed bone unites both superior and inferior endplates through the cage cavities. Previously reported biomechanical changes associated with graft stiffness [9] or contact area [12] alone do not account for contact changes between the implant and the endplates. This change in contact has, so far, not been modelled and its impact on load-distribution pathways may be significant.

In this FE investigation we use a standalone XLIF model to investigate temporal graft maturation, leveraging natural stabilising spinal structures, such as ligaments and facets, to examine its impact on adjacent levels. A holistic approach to the assessment of the region's load-transfer mechanisms would be expected to provide a broader range of clinically meaningful data quantifying effects beyond the index level. This has the potential to answer outstanding clinically relevant questions about the drivers of degeneration and disease at adjacent segments following LIF surgery.

The purpose of this investigation was to examine the effects of temporal bone graft changes, from soft callus formation to complete fusion, on load-distribution among the cage, graft, and surrounding spinal structures for an L4-L5 XLIF using FE analysis.

**Method**

*Image Segmentation and Model Generation from Computed Tomography Data*

High-resolution thoracolumbosacral spine Computed Tomography (CT) data (1291 axial cuts, 512 × 512 pixel resolution, 0.30mm slice thickness) from an anonymised asymptomatic male subject (55 years old) were obtained in DICOM (Digital Imaging and Communications in Medicine) file format from Southern Radiology Miranda (Sydney, Australia). The CT data were imported into Materialise Mimics image processing software (Materialise NV 2018b) for segmentation into anatomical regions of interest for L1-S1.
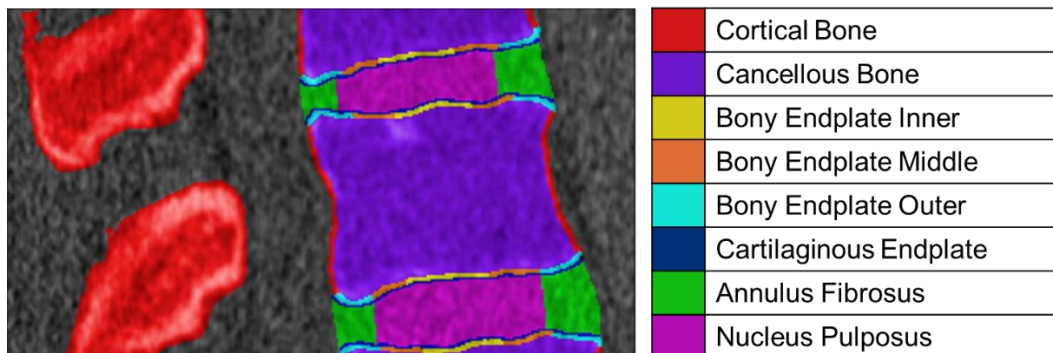


*Figure 1: CT scan segmentation into 8 anatomical regions of interest.*

The nucleus pulposus was assumed to occupy 43% of the total intervertebral disc volume [13]. Further segmentation was undertaken on the annulus fibrosus into five regions for ease of assigning regional stiffness variation according to Schmidt et al. (2006) [14]. Similarly, the bony endplates were modelled for stiffness variation in three regions according to Denoziére & Ku (2006) with equal radial width and thickness of 0.6mm [15]. The cartilage endplate was segmented with a thickness of 0.3mm [16].

The segmented regions were digitally stitched to produce a surface mesh of 3-noded triangle elements in Materialise 3-Matic (Materialise NV _____). The 3D model file (STL) of the XLIF cage (22 x 50 x

10mm, 0° lordosis) was imported into the meshing software and embedded within the L4-L5 intervertebral space using a Boolean operation. Subsequent re-meshing and triangle quality adjustment enabled successful 3D volumetric mesh generation. The 3D volumetric mesh was imported in Nastran file format (.nas) into Strand7 (vers. 2.4.6, Strand7 Pty. Ltd., Sydney, Australia) FE modelling software for pre-processing.

*Modelling Temporal Graft Stiffness Changes*

Two states of contact were modelled between the L4 inferior endplate and superior cage and graft surface. Unbonded contact represented immature fusion progression and incomplete union between the two surfaces, which was modelled using *Normal Contact* elements in Strand7 that allowed for simultaneous lift-off and compressive contact on different regions of the superior cage surface during simulated bending motions. Bonded contact represented bony union through the cage-graft construct, from the L4 inferior endplate to the L5 superior endplate. Five unique graft stiffnesses were modelled in the unbonded state. Two unique graft stiffnesses were modelled in the bonded state.

Graft material variation in the unbonded state represented temporal stiffening from the soft callus (SC) formation stage to a solid graft state, simulated with silicone and poly(methyl methacrylate) (PMMA) respectively. 25% (St1), 50% (St2), and 75% (St3) stiffening were modelled as temporal stages between the two endpoints, whose material properties were obtained using a unit cell approach. With a paucity of information on *in vivo* fusion bone mechanical properties, cancellous bone (Canc.) and cortical bone (Cort.) were modelled in the graft region in the bonded contact state as clinically representative cases of solid bony fusion.
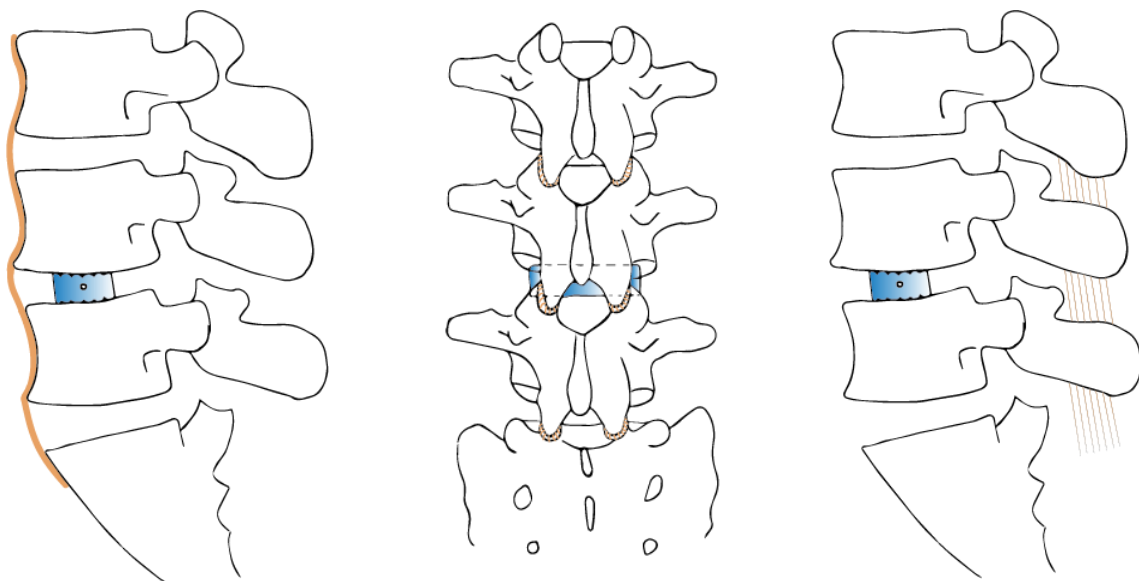


*Figure 1: Anterior longitudinal ligaments (left image); Capsular liagments (middle); and interspinous liagemnts (right)*

*Modelling Annulus Fibres and Ligaments*

The annulus fibrosus was modelled per previously published protocols as a bi-phasic structure of concentric layers (n = 4) of criss-cross collagen fibres embedded within a ground substance [17]. The ends of the fibres were rigidly anchored in the superior and inferior endplates and concentric fibre layers were connected via interlamellar bridges. Annulus fibres were modelled with varying orientation, gradually increasing from ±24° ventrally to ±46° dorsally according to published anatomical data [14]. Ligaments were modelled as cylindrical beam elements, with attachment and insertion sites in accordance with previous protocols and published literature [17, 18].
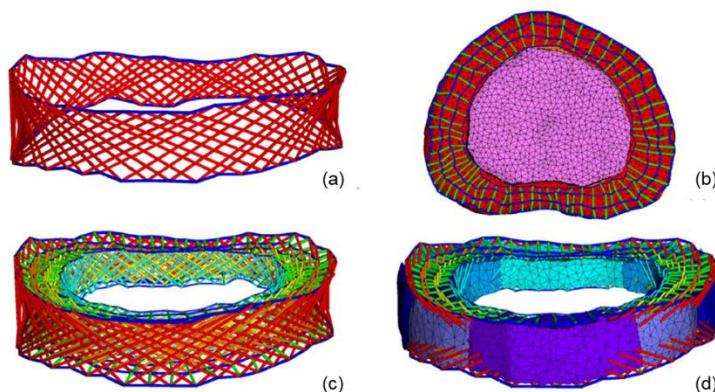


*Figure 2: Annulus fibrosus modelled as a bi-phasic structure with criss-cross collagen fibres embedded within a ground substance.*

*Modelling Facet Joint Articulation*

Compressive load transfer characteristics between facet joints at the bony articulating pillars were modelled by *Point Contact – Tension* elements (n = 5 per joint) in Strand7. The contact elements were evenly distributed over the articulating faces and normally oriented.

*Loads and Boundary Constraints*

A node on the anterior surface of the sacrum, below the sacral promontory, was constrained in all translational and rotational degrees of freedom. Bending moments were applied to the model using a crossbeam construct at the L1 superior endplate, mounted on a surface cap. The surface cap and crossbeam were assigned material properties of structural steel (E = 200GPa, v = 0.25). A force couple was applied to the anterior and posterior extremities of the crossbeam, loading the models in flexion and extension bending. The models were loaded in a stepwise manner with pure unconstrained moments from 1Nm to 10Nm and solved for geometric, material, and boundary nonlinearities using the *Nonlinear Static Solver* in Strand7.

**Results**

*Loading of Interbody Cage*

In both flexion (Fx) and extension (Ex), compressive stress on the interbody cage reduced by 20% with increasing graft stiffness from the SC to PMMA stage in the unfused case (Fx: 0.86MPa (SC) to 0.69MPa (PMMA); Ex: 1.01MPa (SC) to 0.81MPa (PMMA)). Cage stress increased, however, after complete fusion with both cancellous and cortical grafts (Fx: 1.47MPa (Canc.), 1.22MPa (Cort.); Ex: 1.53MPa (Canc.), 1.31MPa (Cort.)).

Stress accounts for change both in area and force. As such, change in compressive force is reported normalised to the SC bone graft model, accounting both for change in the compressive stress and change in the area under compressive stress. Progressive off-loading of the cage was observed with stiffening graft, simulating advancing fusion, from SC to PMMA in flexion only (St1: -18%, St2: -31%, St3: -39%, PMMA: -42%). Modelling of complete fusion increased normalised force in both fused contact models (Fx: 55% (Canc.), 16% (Cort.); Ex: 47% (Canc.), 28% (Cort.)).
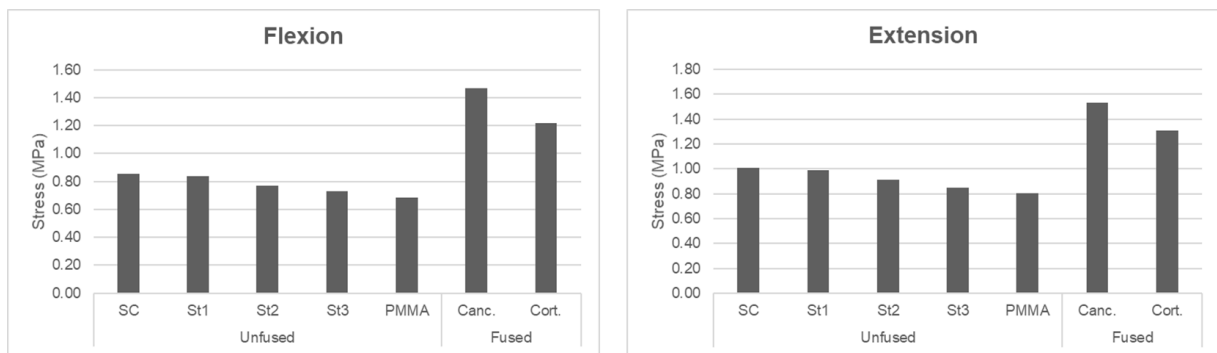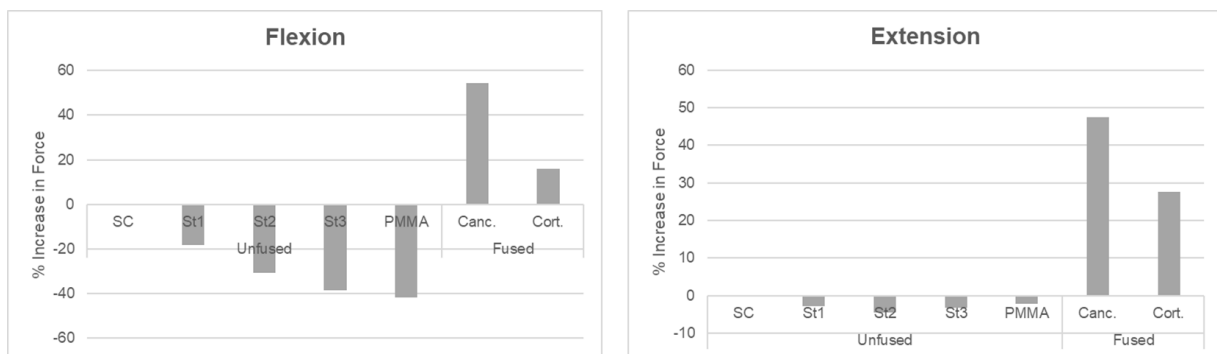


Figure 3: Compressive stress on interbody cage.



Figure 4: Percentage change in compressive force on interbody cage normalised to the SC model.
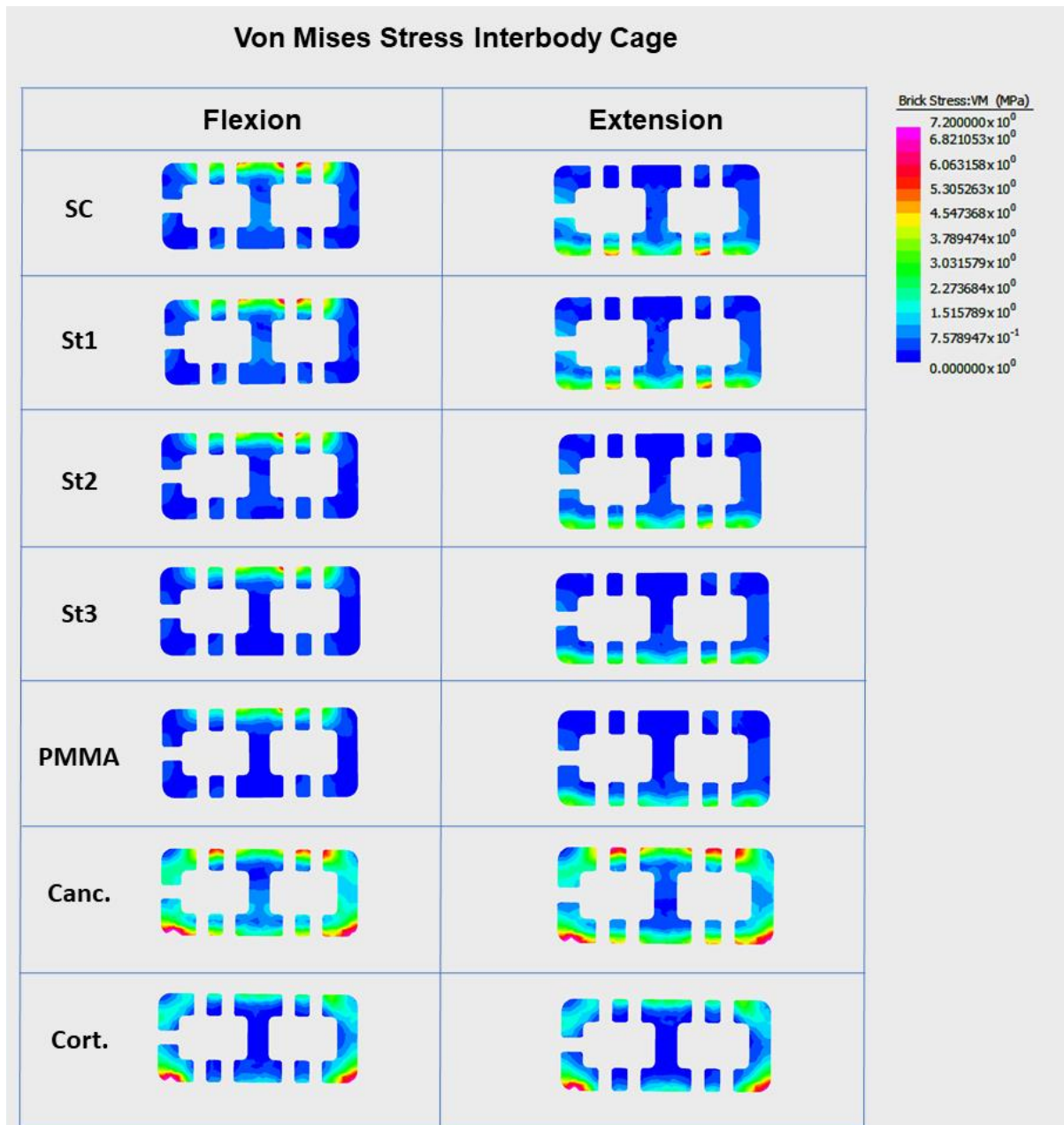
*Figure 5: Von Mises stress on interbody cage in flexion and extension.*

*Loading of Graft*

Compressive graft stress showed an increase associated with graft stiffness in flexion (SC: 0.00MPa, St1: 0.02MPa, St2: 0.09MPa, St3: 0.15MPa, PMMA: 0.22MPa) and extension (SC: 0.00MPa, St1: 0.02MPa, St2: 0.08MPa, St3: 0.14MPa, PMMA: 0.20MPa). Stress on the cancellous bone graft in the fused state was comparable to the 50% stiffening (St2) unbonded model given its similar stiffness properties (Fx: 0.08MPa, Ex: 0.07MPa). A similar trend was observed in normalised compressive force results.
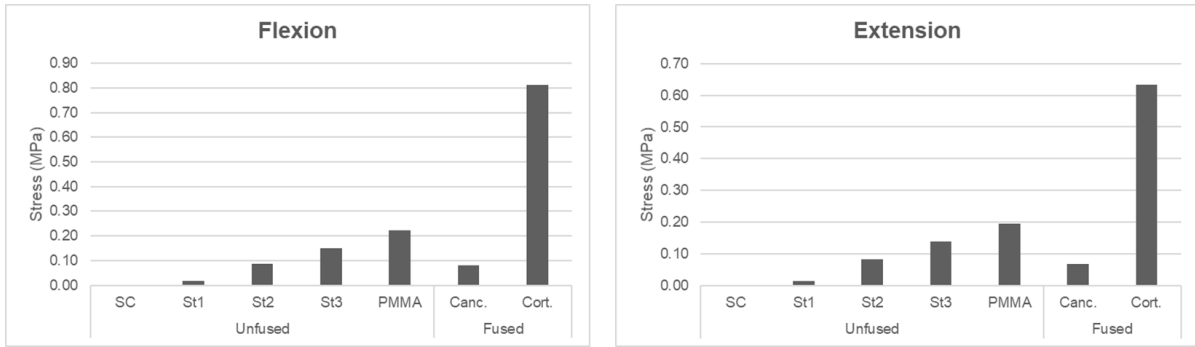
*Figure 6: Compressive stress on graft.*
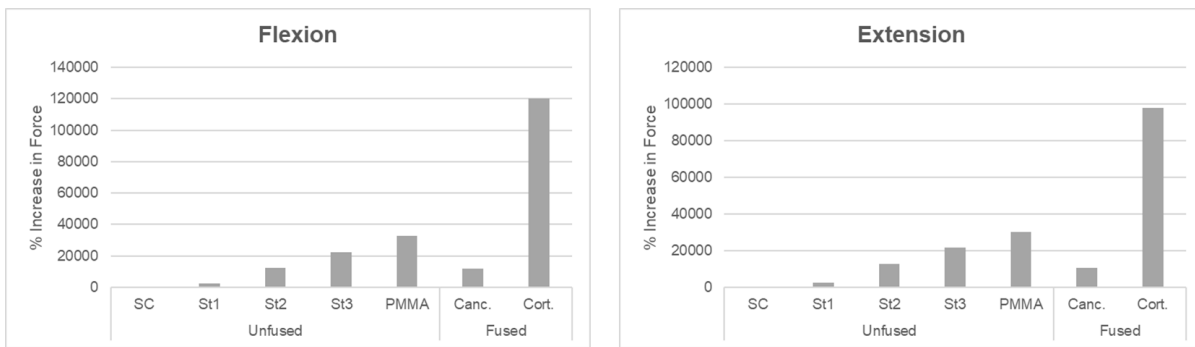


*Figure 7: Percentage change in compressive force on graft normalised to the SC model.*

*Cage:Graft Load-Share*

Increasing graft stiffness improved the compressive load-sharing between the cage and graft as a percentage of total compressive stress on the construct. The SC model exhibited 99.9% stress on the cage (0.1% on graft) in forward and backward bending. The PMMA model showed off-loading of the cage and more stress on the graft in flexion (75.6% cage, 24.4% graft) and extension (80.4% cage, 19.6% graft). Stress-sharing between the cage and graft was associated with graft stiffness and not bonding to the endplates (Fx: 94.7% cage, 5.3% graft (Canc.), 60.0% cage, 40.0% graft (Cort.); Ex: 95.8% cage, 4.2% graft (Canc.), 67.3% cage, 32.7% graft (Cort.)).
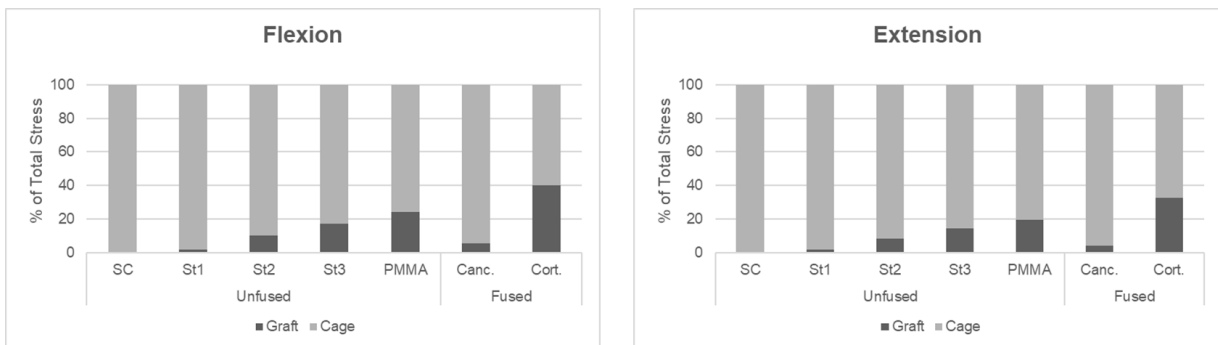


*Figure 8: Compressive stress on cage and graft regions as a percentage of total stress on the construct.*
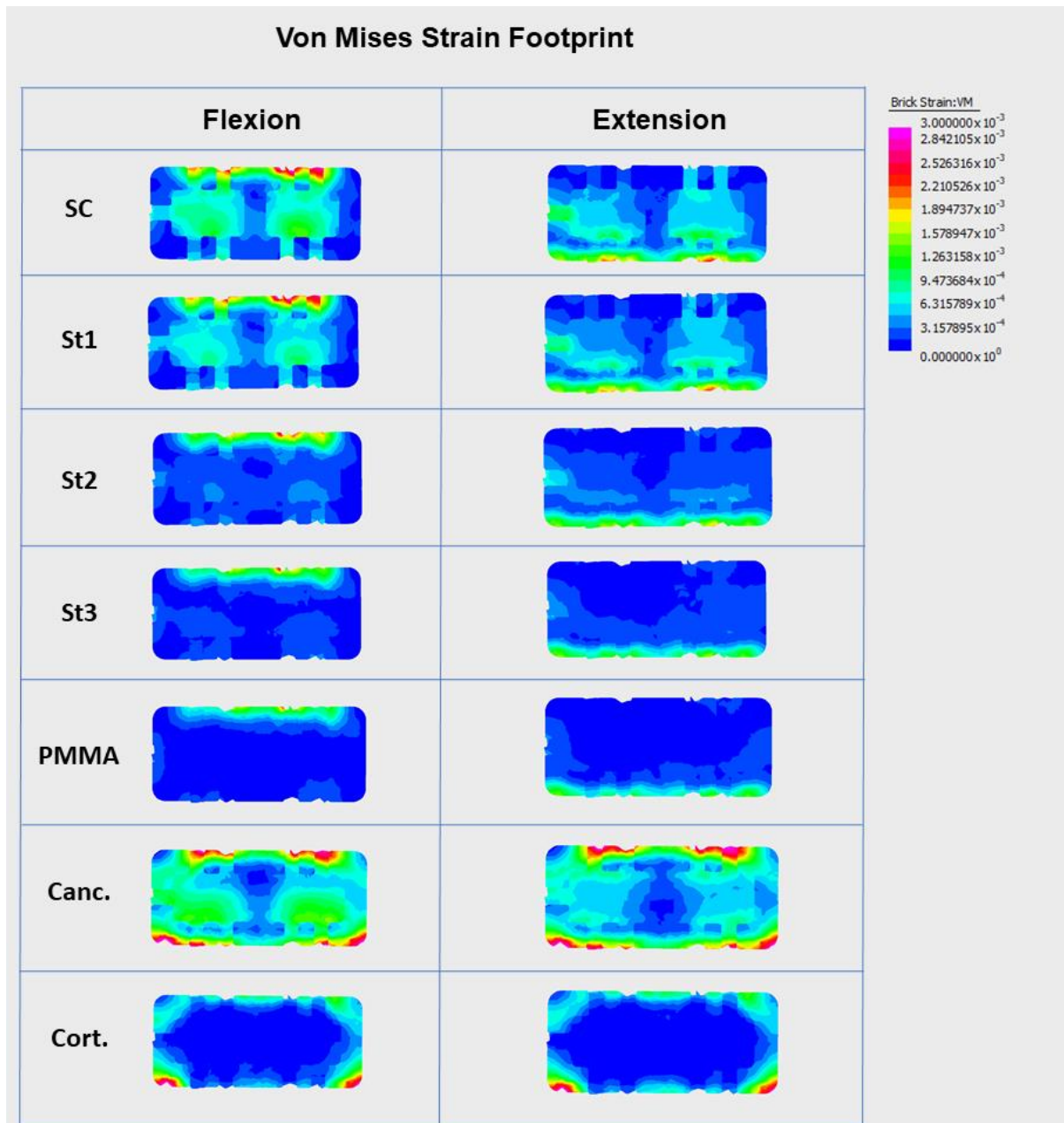
*Figure 9: Von Mises strain of cage-graft footprint in flexion and extension.*

*Cage Anterior Force*

The fused models (Canc., Cort.) exhibited a large increase in anteriorly directed force normalised to the SC stage (Fx: 102% (Canc.), 83% (Cort.); Ex: 97% (Canc.), 67% (Cort.)). Across the unfused models, stiffening of the bone graft reduced anteriorly directed force on the cage. Anterior force decreased by 5%, 21%, 29%, and 33% respectively for St1, St2, St3, and PMMA in flexion compared to SC. Smaller changes were noted in extension (-3% (St1), -6% (St2), -11% (St3), -17% (PMMA)). As with normalised compressive force, normalised anterior force accounted for both change in stress and change in area under anterior stress.

*Figure 10: Percentage change in anteriorly directed force on interbody cage normalised to the SC model.*

*Ligament Strain*

Results from adjacent regions were not significant within the unbonded models (SC, St1, St2, St3, PMMA) and bonded models (Canc., Cort.). In reporting results for ligaments, facets, and intervertebral disc, the pertinent comparison is between the fused and unfused states, which are reported as averages of their respective groups.

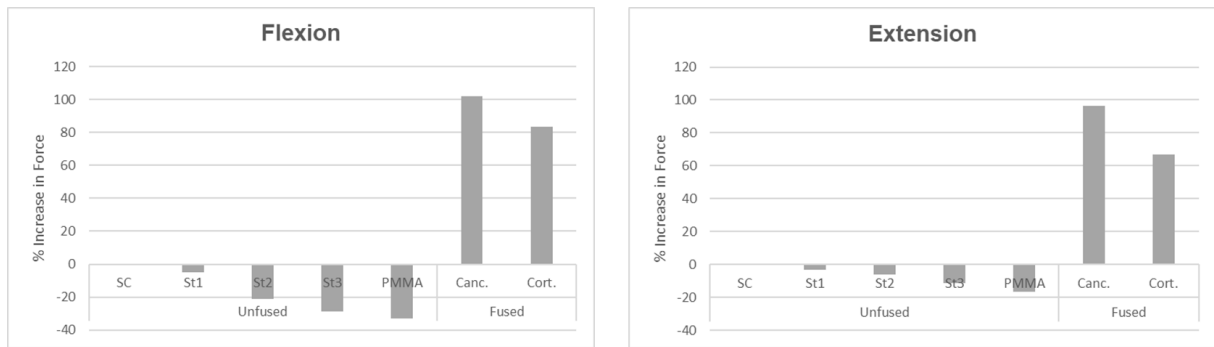The posterior ligaments showed reduced strain at the index level during flexion. They did not exhibit tensile strain in extension. In the fused models, the strain in the ligamentum flavum (LF), interspinous ligament (ISL), and supraspinous ligament (SSL) was reduced at the L4-L5 level by 70%, 63%, and 66% respectively compared to unfused, however changes were insignificant at the adjacent levels. Posterior longitudinal ligament (PLL) strain at L4-L5 of the fused models reduced by 77% in the fused models, accompanied by a decrease of 15% at L4 and 37% at L5. Similarly, for the anterior longitudinal ligament (ALL) in extension, the fused models demonstrated an 89% reduction in strain at L4-L5 and a 28% and 38% off-loading at L4 and L5, respectively. In flexion, strain in the capsular ligaments (CL) reduced by 70% at the index level with no accompanied change at L3-L4 or L5-S1 for solid fusion. In extension, CL were off-loaded at L4-L5 by 97%, however there was a 23% increase in CL strain at L3-L4. No significant change was observed at L5-S1.

*Table 1: Posterior ligament strain in flexion at the level above the XLIF.*

| | Level Above | | | | | | |
|---|---|---|---|---|---|---|---|
| | **Unfused** | | | | | **Fused** | |
| | **SC** | **St1** | **St2** | **St3** | **PMMA** | **Canc.** | **Cort.** |
| **PLL** | 0.00038 | 0.00038 | 0.00038 | 0.00038 | 0.00038 | 0.00032 | 0.00032 |
| **LF** | 0.07525 | 0.07525 | 0.07525 | 0.07525 | 0.07525 | 0.07526 | 0.07526 |
| **ISL** | 0.22422 | 0.22422 | 0.22422 | 0.22421 | 0.22421 | 0.22322 | 0.22322 |
| **SSL** | 0.09735 | 0.09735 | 0.09734 | 0.09734 | 0.09734 | 0.09676 | 0.09676 |
| **CL** | 0.20312 | 0.20312 | 0.20312 | 0.20312 | 0.20312 | 0.20307 | 0.20309 |

*Table 2: Posterior ligament strain in flexion at the level of the XLIF.*

| | Index Level | | | | | | |
|---|---|---|---|---|---|---|---|
| | Unfused | | | | | Fused | |
| | SC | St1 | St2 | St3 | PMMA | Canc. | Cort. |
| PLL | 0.04982 | 0.04982 | 0.04980 | 0.04978 | 0.04977 | 0.01165 | 0.01105 |
| LF | 0.06073 | 0.06072 | 0.06068 | 0.06065 | 0.06061 | 0.01858 | 0.01774 |
| ISL | 0.20110 | 0.20104 | 0.20078 | 0.20061 | 0.20046 | 0.07574 | 0.07219 |
| SSL | 0.07947 | 0.07944 | 0.07929 | 0.07919 | 0.07911 | 0.02799 | 0.02667 |
| CL | 0.15734 | 0.15734 | 0.15733 | 0.15727 | 0.15721 | 0.04891 | 0.04686 |

*Table 3: Posterior ligament strain in flexion at the level below the XLIF.*

| | Level Below | | | | | | |
|---|---|---|---|---|---|---|---|
| | Unfused | | | | | Fused | |
| | SC | St1 | St2 | St3 | PMMA | Canc. | Cort. |
| PLL | 0.00037 | 0.00037 | 0.00038 | 0.00038 | 0.00038 | 0.00023 | 0.00024 |
| LF | 0.11385 | 0.11385 | 0.11386 | 0.11387 | 0.11387 | 0.11346 | 0.11351 |
| ISL | 0.23075 | 0.23075 | 0.23076 | 0.23077 | 0.23078 | 0.22997 | 0.23006 |
| SSL | 0.14063 | 0.14063 | 0.14064 | 0.14064 | 0.14065 | 0.13970 | 0.13977 |
| CL | 0.16443 | 0.16444 | 0.16447 | 0.16448 | 0.16449 | 0.16421 | 0.16433 |

*Table 4: ALL and CL strain during extension at level above the XLIF.*

| | Level Above | | | | | | |
|---|---|---|---|---|---|---|---|
| | Unfused | | | | | Fused | |
| | SC | St1 | St2 | St3 | PMMA | Canc. | Cort. |
| ALL | 0.00142 | 0.00142 | 0.00142 | 0.00142 | 0.00142 | 0.00102 | 0.00103 |
| CL | 0.01928 | 0.01928 | 0.01928 | 0.01928 | 0.01928 | 0.02366 | 0.02373 |

*Table 5: ALL and CL strain during extension at level of the XLIF.*

| | Index Level | | | | | | |
|---|---|---|---|---|---|---|---|
| | Unfused | | | | | Fused | |
| | SC | St1 | St2 | St3 | PMMA | Canc. | Cort. |
| ALL | 0.04533 | 0.04533 | 0.04533 | 0.04533 | 0.04534 | 0.00515 | 0.00478 |
| CL | 0.03776 | 0.03777 | 0.03786 | 0.03792 | 0.03797 | 0.00115 | 0.00091 |

*Table 6: ALL and CL strain during extension at level below the XLIF.*

| | Level Below | | | | | | |
|---|---|---|---|---|---|---|---|
| | Unfused | | | | | Fused | |
| | SC | St1 | St2 | St3 | PMMA | Canc. | Cort. |
| ALL | 0.00155 | 0.00155 | 0.00154 | 0.00154 | 0.00154 | 0.00096 | 0.00097 |
| CL | 0.12591 | 0.12590 | 0.12592 | 0.12593 | 0.12595 | 0.12745 | 0.12744 |

*Facet Axial Force*

Axial force results from the facets represent the compressive load-transfer capabilities of the joint. In flexion, no compressive load transfer was noted in fused models at L4-L5 through the facets. L3-L4 axial force was reduced by 11% and no significant change was observed at L5-S1. Compressive load through L4-L5 during extension was reduced by 87% due to solid fusion with no significant changes at adjacent facets.

*Table 7: Axial force on facets at the level above, index level, and level below in N.*

| | | Unfused | | | | | Fused | |
|---|---|---|---|---|---|---|---|---|
| | | SC | St1 | St2 | St3 | PMMA | Canc. | Cort. |
| Level Above | Fx | 2.71594 | 2.71558 | 2.71430 | 2.71331 | 2.71245 | 2.42605 | 2.42001 |
| | Ex | 12.13871 | 12.13858 | 12.13816 | 12.13786 | 12.13759 | 11.87338 | 11.87134 |
| Index Level | Fx | 1.33717 | 1.33676 | 1.34271 | 1.35281 | 1.36503 | 0.00000 | 0.00000 |
| | Ex | 11.02500 | 11.02230 | 11.01988 | 11.01653 | 11.01249 | 1.44737 | 1.36951 |
| Level Below | Fx | 1.86622 | 1.86566 | 1.86441 | 1.86374 | 1.86322 | 2.00479 | 1.99816 |
| | Ex | 4.67596 | 4.67646 | 4.67925 | 4.68129 | 4.68288 | 4.72035 | 4.72667 |

*Adjacent Intervertebral Discs Normal Stress*

Changes in normal stress at the L3-L4 and L5-S1 intervertebral discs were largely insignificant when comparing the fused and unfused models. The largest changes observed were at the L3-L4 annulus and nucleus (3% and 2% increase with fusion, respectively) and L5-S1 annulus (2% increase with fusion) in extension.

*Table 8: L3-L4 intervertebral disc compressive stress in MPa.*

| | | Unfused | | | | | Fused | |
|---|---|---|---|---|---|---|---|---|
| | | SC | St1 | St2 | St3 | PMMA | Canc. | Cort. |
| AF | Fx | 0.10702 | 0.10703 | 0.10704 | 0.10704 | 0.10704 | 0.10824 | 0.10821 |
| | Ex | 0.10445 | 0.10445 | 0.10446 | 0.10445 | 0.10445 | 0.10757 | 0.10763 |
| NP | Fx | 1.14140 | 1.14140 | 1.14158 | 1.14160 | 1.14162 | 1.14572 | 1.14571 |
| | Ex | 1.06583 | 1.06585 | 1.06589 | 1.06592 | 1.06594 | 1.08558 | 1.08572 |

*Table 9: L5-S1 intervertebral disc compressive stress in MPa.*

| | | Unfused | | | | | Fused | |
|---|---|---|---|---|---|---|---|---|
| | | SC | St1 | St2 | St3 | PMMA | Canc. | Cort. |
| AF | Fx | 0.06878 | 0.06878 | 0.06876 | 0.06875 | 0.06875 | 0.06938 | 0.06936 |
| | Ex | 0.28386 | 0.28384 | 0.28384 | 0.28386 | 0.28388 | 0.28873 | 0.28870 |
| NP | Fx | 1.21624 | 1.21628 | 1.21646 | 1.21646 | 1.21644 | 1.22822 | 1.22783 |
| | Ex | 0.97860 | 0.97849 | 0.97863 | 0.97859 | 0.97855 | 0.98455 | 0.98483 |

**Discussion**

The main objective of this FE analysis was to investigate the biomechanical changes resulting from temporal graft stiffness changes in a L4-L5 XLIF. Previous studies have demonstrated the higher stresses present in stiffer bone grafts [8, 9], however the load-sharing ratio between cage and graft and consequent changes to load-distribution pathways at adjacent levels has not previously been quantified. Furthermore, this suite of FE models accounts for changes in the mechanical properties of the graft in addition to the progression from unfused to fused contact.

Across the fused and unfused states, results showed that graft stiffness influences the strain distribution at the implant-endplate interface, or cage footprint. Agarwal et al. (2013) detail the effect that an even stress distribution across the endplates may have on cage subsidence [19]. Stress risers on the cage surface are likely to increase the risk of subsidence [19]. Hence, even cage footprints are desirable in lumbar interbody fusion surgeries. Progressive off-loading of the cage (25% Fx, 20% Ex) and increased loading on the graft favourably redistributed stress across the cage footprint as the graft stiffened from the SC to PMMA stage. Similarly, cortical bone (Cort.) produced a more even footprint than the cancellous model (Canc.). As fusion progressed, Von Mises (VM) stress plots indicated a noticeable stress reduction in the central region of the interbody cage aligned with the softest region of the endplates [20].

Despite progression to complete fusion, force through the graft remained stiffness-dependent. The cancellous graft bore 5% of total compressive stress in flexion and 4% in extension, comparable to a stiffness stage between St1 and St2. Cortical fusion bone, however, absorbed 40% of compressive stress in flexion and 33% in extension. Evidently, the requisite to shift the load-sharing ratio towards the theoretically ideal value, based on the proportional area of the graft and cage, was a significantly stiffer fusion mass. Cortical bone modulus is 3-7 times higher than that of PEEK and approximately 80 times higher than the cancellous bone material used in this model [21]. Notwithstanding the influence of bone quality on subsidence risk [22], it is clear that increasing graft stiffness impacts the cage footprint and load-distribution through the cage-graft construct in a manner that reduces the likelihood of stress risers on the cage and subsequent subsidence. Whether the fusion mass is likely to reach a stiffness as high as cortical bone remains debatable and subject to *in vivo* research.

The unfused models experienced a reduction in anteriorly directed forces with increasing graft modulus in flexion (-33% from SC to PMMA) and extension (-17% from SC to PMMA). Although the fused models showed an average increase in anterior force compared to unfused, after solid fusion the onset of instability-related conditions is unlikely. This outcome, however, was not unexpected given the complete bonding of the surfaces. Regardless, the understanding of anterior forces with

respect to temporal fusion progression in its early stages is relevant to the post-operative management of a standalone XLIF and decisions on supplemental fixation.

Compressive force results confirmed that after bony fusion more load passes through the cage. With bonded contact, ligament axial strains also showed a significant reduction in load transferred through the LF, ISL, and SSL at the level of the fusion in flexion. Further reductions were noted in the PLL (Fx) and ALL (Ex) at L4-L5 and adjacent levels. The CL, which are responsible for tensile force transfer at the facets, were off-loaded in flexion and extension at L4-L5, however CL strain increased at L3-L4 during extension. Less compressive force was measured through the facets at L4-L5 in both bending motions with respect to the unfused state. L3-L4 facets were also off-loaded in flexion. No changes were observed to loads in the adjacent discs. Regardless of the mechanical properties of the fusion mass, it is evident that after complete bonding is achieved, more load passes through the cage and less load is transferred through ligaments and facets.

The results suggest that fused contact between the cage-graft complex and the adjacent endplates shifts load-distribution pathways from the ligaments and facets to the implant in a standalone XLIF. Where the fused bone is comparable to cancellous bone, the stiffness may not be high enough to share the load with the cage and suitably balance the load transfer. The substantial graft stiffening in the cortical bone model improved load-share between the cage and graft, however load-distribution changes did not extend to the other spinal structures. The purpose of standalone XLIF is to preserve the stabilising capacity of surrounding ligaments and facets, providing minimal disruption to the natural load-transfer mechanisms of the spine [1]. These results suggest that once complete fusion is achieved, these existing load paths are seemingly diminished.

Such alterations in the load-distribution have implications for rehabilitation advice in the early stages of bone formation after LIF surgery. Furthermore, in the comparison of complete fusion and the unfused states, the results do not suggest an increased likelihood of adjacent segment degeneration stemming from increased loading. Despite the fused contact from L4 to L5, only the L3-L4 CL showed an increase in loading in extension where all other adjacent structures were off-loaded or showed no change.

Future research should focus on a comparison between intact and XLIF surgery models to determine whether changes at adjacent levels are likely to cause adjacent segment degeneration before the commencement of fusion bone formation. While results from this FE analysis have shown that subsidence risk may decrease with graft stiffness, further research should ascertain whether this assertion remains valid across different states of bone quality.

Some modelling limitations were noted in this study. Firstly, the contact between the cage-graft bottom surface and L5 superior endplate was bonded. Contact changes were modelled at the implant top surface and L4 inferior endplate. Furthermore, contact modelling was limited by insufficient data on friction coefficients for the interfacing materials. To the best of our knowledge, there is no published data examining the mechanical properties of *in vivo* fusion bone. As such, modelling the stiffness properties was challenging and relied on existing properties for cancellous and cortical bone in the fused states. Lastly, only four layers of collagen fibres were modelled within the annulus fibrosus with superior and inferior interlamellar bridges, but no translamellar bridges throughout the height of the annulus.

**Conclusions**

Temporal stiffening of the graft in the early stages of bone formation prior to bony fusion causes a shift in load from the cage onto the graft and a reduction in anteriorly directed forces. Full bony union between the endplates elicits a re-distribution of load from the ligaments and facets to the implant.

**Acknowledgements**

**References**

1. Malham, G.M., et al., *Maintenance of Segmental Lordosis and Disk Height in Stand-alone and Instrumented Extreme Lateral Interbody Fusion (XLIF).* Clin Spine Surg, 2017. **30**(2): p. E90-E98.
2. Ozgur, B.M., et al., *Extreme Lateral Interbody Fusion (XLIF): a novel surgical technique for anterior lumbar interbody fusion.* Spine J, 2006. **6**(4): p. 435-43.
3. Cappuccino, A., et al., *Biomechanical analysis and review of lateral lumbar fusion constructs.* Spine (Phila Pa 1976), 2010. **35**(26 Suppl): p. S361-7.
4. Chen, E., et al., *Cage Subsidence and Fusion Rate in Extreme Lateral Interbody Fusion with and without Fixation.* World Neurosurg, 2019. **122**: p. e969-e977.
5. Dominguez, I., et al., *Extreme lateral lumbar interbody fusion. Surgical technique, outcomes and complications after a minimum of one year follow-up.* Rev Esp Cir Ortop Traumatol, 2017. **61**(1): p. 8-18.
6. Epari, D.R., F. Kandziora, and G.N. Duda, *Stress shielding in box and cylinder cervical interbody fusion cage designs.* Spine (Phila Pa 1976), 2005. **30**(8): p. 908-14.
7. Frost, H.M., *Wolff's Law and bone's structural adaptations to mechanical usage: an overview for clinicians.* Angle Orthod, 1994. **64**(3): p. 175-88.
8. Rohlmann, A., T. Zander, and G. Bergmann, *Effects of fusion-bone stiffness on the mechanical behavior of the lumbar spine after vertebral body replacement.* Clin Biomech (Bristol, Avon), 2006. **21**(3): p. 221-7.
9. Zander, T., et al., *Effect of bone graft characteristics on the mechanical behavior of the lumbar spine.* J Biomech, 2002. **35**(4): p. 491-7.
10. Vadapalli, S., et al., *Biomechanical rationale for using polyetheretherketone (PEEK) spacers for lumbar interbody fusion-A finite element study.* Spine (Phila Pa 1976), 2006. **31**(26): p. E992-8.
11. Du, L., et al., *The role of cage height on the flexibility and load sharing of lumbar spine after lumbar interbody fusion with unilateral and bilateral instrumentation: a biomechanical study.* BMC Musculoskelet Disord, 2017. **18**(1): p. 474.
12. Steffen, T., et al., *Cages: designs and concepts.* Eur Spine J, 2000. **9 Suppl 1**: p. S89-94.
13. White, A.A. and M.M. Panjabi, *Clinical biomechanics of the spine*. 2nd ed. 1990, Philadelphia, PA: JB Lippincott.
14. Schmidt, H., et al., *Application of a new calibration method for a three-dimensional finite element model of a human lumbar annulus fibrosus.* Clin Biomech (Bristol, Avon), 2006. **21**(4): p. 337-44.
15. Denoziere, G. and D.N. Ku, *Biomechanical comparison between fusion of two vertebrae and implantation of an artificial intervertebral disc.* J Biomech, 2006. **39**(4): p. 766-75.
16. Roberts, S., J. Menage, and J.P. Urban, *Biochemical and structural properties of the cartilage end-plate and its relation to the intervertebral disc.* Spine (Phila Pa 1976), 1989. **14**(2): p. 166-74.

17. Ramakrishna, V.A.S., et al., *The Role of Sacral Slope in the Progression of a Bilateral Spondylolytic Defect at L5 to Spondylolisthesis: A Biomechanical Investigation Using Finite Element Analysis.* Global Spine J, 2018. **8**(5): p. 460-470.

18. Behrsin, J.F. and C.A. Briggs, *Ligaments of the lumbar spine: a review.* Surg Radiol Anat, 1988. **10**(3): p. 211-9.

19. Agarwal, A., et al., *Biomechanical evaluation of an endplate-conformed polycaprolactone-hydroxyapatite intervertebral fusion graft and its comparison with a typical nonconformed cortical graft.* J Biomech Eng, 2013. **135**(6): p. 61005-9.

20. Edwards, W.T., et al., *Structural features and thickness of the vertebral cortex in the thoracolumbar spine.* Spine (Phila Pa 1976), 2001. **26**(2): p. 218-25.

21. Lu, Y.M., W.C. Hutton, and V.M. Gharpuray, *Do bending, twisting, and diurnal fluid changes in the disc affect the propensity to prolapse? A viscoelastic finite element model.* Spine (Phila Pa 1976), 1996. **21**(22): p. 2570-9.

22. Polikeit, A., et al., *The importance of the endplate for interbody cages in the lumbar spine.* Eur Spine J, 2003. **12**(6): p. 556-61.